ADVANCED FUNCTIONAL MATERIALS
www.afm-journal.de

Exploiting the Base-Triggered Thiol/Vinyl Ether Addition to Prepare Well-Defined Microphase Separated Thermo-Switchable Adhesives

Aritz Lamas, Lucas Polo Fonseca, Cécile Moussard, Daniela de Morais Zanata, Gabriel Perli, Marta Ximenis, Xabier Lopez de Pariza, Guillem Seychal, Marco Caliari, Miren Itxaso, Robert Aguirresarobe, Iñigo Calvo, and Haritz Sardon**

Switchable adhesives are materials of utmost importance due to their capability of having their adhesion/cohesion properties reversibly triggered upon stimuli, allowing on-demand surface attaching/detaching. Still, several challenges mainly associated with complex uncontrolled chemical processes hinders their production. In this study, it is found that unexpectedly vinyl ethers are able to react with thiols in the presence of a catalytic concentration of base, which allows the preparation of well-defined phase-separated switchable adhesives. Indeed, these findings show that base-catalyzed thiol-acrylate and thiol-vinyl ether are highly orthogonal, making the acrylate reaction faster. This is explored to react in the first stage thiols with acrylates in the presence of vinyl ethers to end-cap all the oligomers with stable vinyl ethers and suppress undesirable disulfide formation. In a second stage the UV-triggered thiol-ene "click reaction" is carried out, forming the network. It is shown that the network prepared by this approach presents superior adhesion due to greater backbone length, a controlled crosslinking motif, and better-defined microphase separation. Additionally, the adhesives made by this strategy are thermo-switchable due to the temperature-triggered base-catalyzed thioether dynamic covalent character at 200 °C. Despite providing superior adhesive properties, the proposed technology endows scalable, thermo-switchable, and O_2-resistant adhesives with huge industrialization potential.

1. Introduction

Synthetic polymeric adhesives are materials used to bind distinct surfaces for a vast plethora of applications since the discovery of phenolic resins in the early 20th century.[1] Most recently, the need for adhesives that can attach/detach surfaces selectively and on-demand upon external stimuli has arisen due to its environmental advantage of enabling several cycles of use/reuse.[2–6] Furthermore, the possibility of selective triggering bonding/de-bonding allows for recovering/re-using expensive automotive, electronic, or aerospatial components by allowing adhesive removal without damaging the parts.

The adhesion between substrates derives from strong intermolecular interactions between the adhesive and both substrate surfaces, while the adhesive strength and resistance to shear are related to the polymer cohesive energy density, referred to as simply cohesion.[7,8] As the crosslinking density of a polymer increases, the polymer's cohesion also increases due to the higher density of covalent bonds.

A. Lamas, L. Polo Fonseca, C. Moussard, D. de M. Zanata, G. Perli, M. Ximenis, X. Lopez de Pariza, G. Seychal, M. Caliari, M. Itxaso, R. Aguirresarobe, H. Sardon
POLYMAT
University of the Basque Country UPV/EHU
Joxe Mari Korta Center, Avda Tolosa 72, Donostia-San Sebastian 20018, Spain
E-mail: lucas.polodafonseca@ehu.eus; haritz.sardon@ehu.eus

The ORCID identification number(s) for the author(s) of this article can be found under https://doi.org/10.1002/adfm.202412584

DOI: 10.1002/adfm.202412584

M. Caliari
Center for Education and Research on Macromolecules (CERM)
CESAM Research Unit
University of Liege
Sart-Tilman B6a, Liege 4000, Belgium

I. Calvo
ORIBAY Group Automotive S.L. R&Department
Donostia-San Sebastián 20018, Spain

I. Calvo
Laboratory of Polymeric and Composite Materials
Center of Innovation and Research in Materials and Polymers (CIRMAP)
University of Mons
Place du Parc 23, Mons 7000, Belgium

However, this increase in crosslinking density can decrease adhesion. Therefore, alternative methods to enhance adhesive cohesion are often explored.[8] Among the several strategies to increase adhesive cohesion without decreasing its adhesion is to achieve microphase-separation in the adhesives. Such morphologies comprise distinct phases of distinct mechanical behavior in the micrometer range (<10 μm), enabling the coexistence between soft (high adhesion), and hard (high cohesion) domains within a unique material.[9–13] Microphase-separated morphologies are typically found in polyurethane-based adhesives, due to the presence of hard domains formed by the segments rich in diisocyanate, while soft domains are formed by the generally soft-polyols used in PU manufacturing.[14] Still, polyurethane (PU) faces poor spatial and temporal control over their polymerization, due to isocyanate chemistry,[15] leading to severe manufacturing issues when dealing with pressure-sensitive adhesives. Therefore, alternative microphase-separated adhesives should be investigated where well-defined structures should be targeted. Moreover, those adhesives must fulfill the industrial requirements and cure in a short period of time.

In this direction, advancements in the concept of "click" chemistry and "click" reactions can be of great relevance.[16–18] Among "click" reactions, the thiol-X family of reactions has huge potential due to their potential UV-initiation, and low cost compared to other "click-like" chemistries.[18–21] However, thiol-X "click-like" reactions face severe side-reaction issues when it comes to applying such chemistries for polymerization purposes,[22–24] leading to several authors even questioning the "click-like"-nature of such chemistry. Those side reactions lead to severe shelf-life stability issues and topological heterogeneity on chemical networks which affects the performance of polymeric materials. In the case of the radical catalyzed thiol-ene polymerization, the main side reactions are the concurrent free radical polymerization, and disulfide formation via thiyl radical combination.[24] On the other hand, base-catalyzed thiol-Michael addition polymerization can lead to the formation of disulfides if thiols are left with a base under environmental conditions. This happens due to a water-catalyzed redox mechanism, analogously to typical disulfide formation in typical thiol-containing aminoacids.[25,26] While the concurrent free radical polymerization side-reaction can lead to uncontrolled phase-separation and irreversible chemically crosslinked domains, the disulfide formation may lead to adhesive stiffening.

In this study, we elucidate the conditions in which such side reactions occur and how to avoid/minimize their occurrence to allow us to prepare low-cost, scalable, thermo-switchable pressure sensitive-adhesives by means of sequential thiol-Michael/ene polymerizations (**Figure 1**). After performing a thorough assessment of thiol-Michael/ene polymerizations and their side-reactions, unexpectedly we found that the thiol/vinyl ether reactions occur in the presence of catalytic base concentration which allows us to prepare a stable liquid-liquid phase separated resins that can be post-cured to form microphase separated pressure-sensitive adhesives (PSAs). We demonstrate that getting a well-defined network brings significant enhancement to the adhesion properties. Furthermore, we take advantage of thioether dynamic behavior at $T \geq 200$ °C[27,28] to endow adhesive thermo-switchability. Finally, we leverage the superior O_2 resistance of radical thiol-ene reactions[29] for adhesive formulations, compared to typical acrylic adhesives. By laminating the adhesives in open air, we demonstrate that thiol-ene reactions cure more effectively than conventional free radical polymerization of acrylates. This is impeded by oxygen, which restricts the performance of traditional UV-active acrylic adhesives and creates significant challenges for their use in industrial applications.

2. Results and Discussion

2.1. Thiol-Michael and Thiol-Ene Polymerization Screening

As demonstrated by the groups of professors Bowman,[30–35] and Hoyle[36,37] that have laid the groundwork with outstanding fundamental research regarding thiol-Michael addition and thiol-ene mechanism and high-performance thermosets done by such technologies, depending on the double bond nature, the thiols are able to react radically, anionically or cationically in a highly efficient fashion (**Scheme 1**). However, we miss a precise description of the occurrence, or not, of side reactions on such polymerizations[24] which is essential for fully leveraging the potential of these systems.

To support the effectivity of the sequential thiol-acrylate/-vinyl ether strategy on the preparation of well-defined microphase-separated networks, first, a thorough study regarding the polymerization between dithiols and divinyls to form the precursor linear polymers was conducted.

We started analyzing the base-catalyzed thiol-acrylate Michael-addition polymerization between ethylene glycol dimercaptoacetate (GDMA) and polyethylene glycol diacrylate (PEGda) in presence of 0.1 mol% of 1,8-Diazobicyclo [5.4.0]undec-7-ene (DBU) in respect to thiols (0.001 equiv.) which was expected to be extremely fast (Figure S1, Supporting Information). In fact, within 120 s the system reaches conversion of both thiol and acrylates superior to 99%. However, using an excess of thiols in the first step is problematic, as it leads to rapid disulfide bond formation. This issue persists even under stoichiometric thiol/acrylate or thiol/vinyl ether conditions as verified by the rapid formation (≈30 s) of characteristic disulfide bands in the spectra of Fourier-transformed infra-red spectroscopy (FTIR) at 530, 1218, 1356, and 1700 cm^{-1} (**Figure 2B**).[16,25,26,38] However, the addition of 2 mol% excess of acrylates in the reaction mixture restricted the disulfide formation as determined by both FTIR (Figure 2C) and by proton nuclear magnetic resonance spectroscopy (^{1}H NMR) (Figure S2, Supporting Information). Indeed, The characteristic CH_2-associated peaks adjacent to the disulfides are broad and centered at 3.6 ppm, in contrast with the CH_2 adjacent to the thiol, which is a well-defined duplet that is located at 3.2 ppm, Figure S2 (Supporting Information). No broad peak at 3.6 ppm is verified in the ^{1}H NMR spectra of the model polymerizations when using 2 mol% excess of vinyls with respect to thiols, further confirming the success of such a strategy in suppressing disulfide formation.

Besides, the use of the base catalysis prevents the potential homopolymerization of acrylates in typical radical-initiated thiol-ene formulations as demonstrated when thiol and acrylate polymerization was initiated with a photo radical initiator (Figure S3, Supporting Information). Indeed, while acrylates reached full conversion in <1 min, thiols only reached up to 50–60%

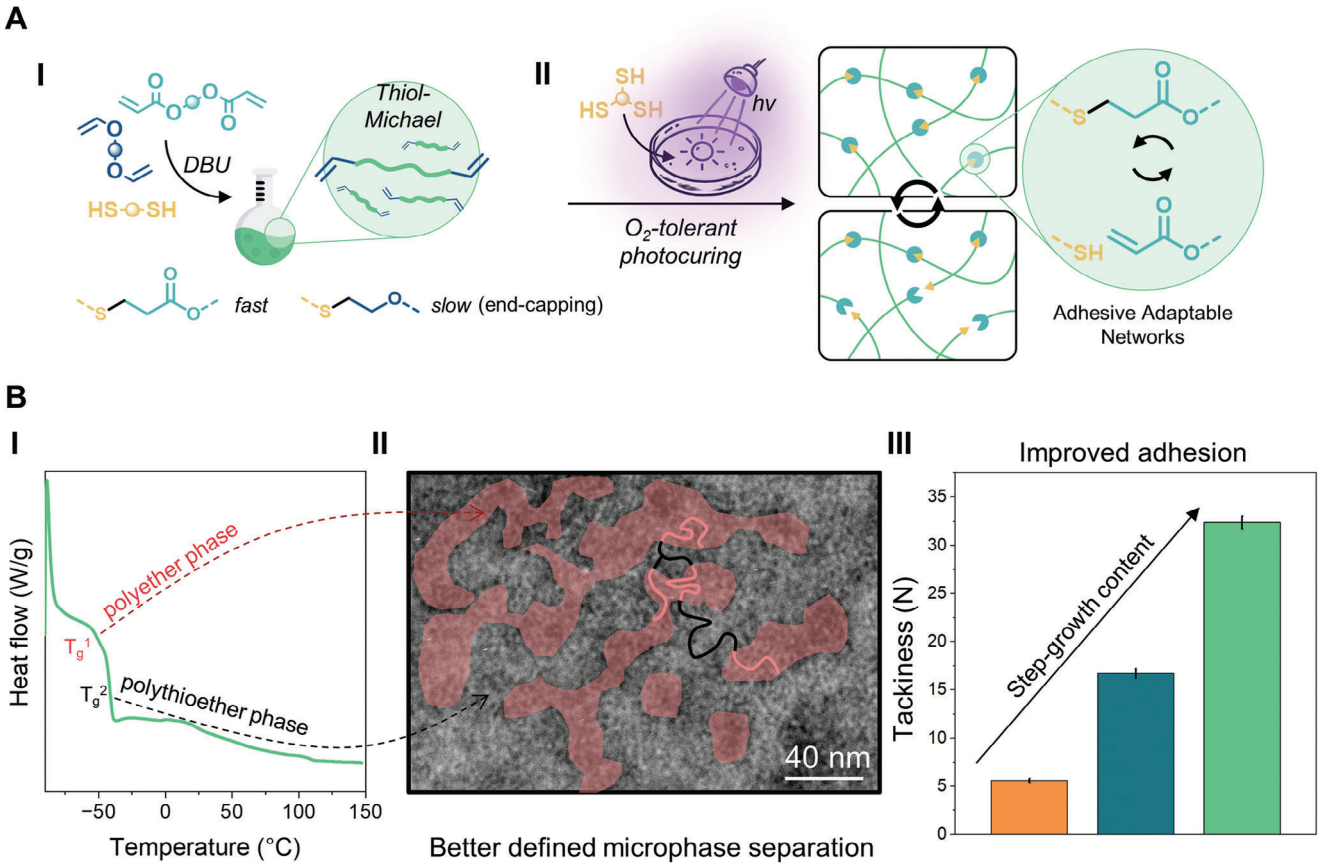

Figure 1. A) Scheme of network produced via side-reaction-free sequential thiol-Michael/ene polymerization developed in this study and of its covalent-adaptable network behavior. B) Differential scanning calorimetry (DSC) second heating scans showing two distinct glass transitions related to distinct phases (I), as shown in magnified TEM image with red-highlighted darker phases (polyether-rich) (II), which leads to improvement in adhesive properties (III).

conversion, strongly suggesting the free-radical polymerization (FRP) of acrylates Figure S3 (Supporting Information).

Then we investigated the base-catalyzed thiol-vinyl ether thiol-Michael addition using the difunctional GDMA dithiol (1 equiv.) and triethylene glycol di(vinyl ether) (TEGdv) (1.02 equiv.) using different amounts of DBU as catalyst (**Figure 3**). Surprisingly we found that 0.1 mol% of DBU was sufficient to promote the reaction at room temperature between vinyl ether groups and thiols, as demonstrated by ^{1}H NMR analysis (Figure 3A; Figures S4 and S5, Supporting Information), but with the selective formation of anti-Markovnikov-type adducts. Previous studies[39] report the occurrence of both Markovnikov and anti-Markovnikov thiol additions to vinyl ethers in the absence of catalysts, with similar mercaptopropionate groups, but at temperatures equal or higher to 100 °C in solvent- and catalyst-free conditions. However, to the best of our knowledge, such room-temperature base-triggered anti-Markovnikov thiol-vinyl ether addition was never reported. The influence of DBU on the selectivity and kinetics of this addition reaction was investigated using 0.1, 1, and 10 mol% of DBU (Figure 3C). Using 1 mol% of DBU the kinetics of the reaction was significantly affected reaching only 35% of conversion in 4 h, while maintaining the selectivity for anti-Markovnikov-type adducts. However, when 10 mol% of DBU was utilized, thiol addition to the vinyl ether did not occur. Conversion was estimated using ^{1}H NMR peak integral values (Figures S4 and S5, Supporting Information) by Equations S2 and S3 (Supporting Information). In order to confirm that increasing the proportion of DBU hinders the thiol addition to vinyl ether, we conducted a model reaction using butyl vinyl ether and butyl thiol. Both were present in equimolar amounts along with DBU, at room temperature and at 80 °C (refer to Figures S6–S9, Supporting Information). However, no reaction occurred under either condition, as verified by ^{1}H NMR, in which the peak-integral values for the reactants, before and after mixing and heating at 80 °C for 6 h, remain the same, Figure S9 (Supporting Information).

Importantly, in a prior study, Lin and colleagues[40] verified highly selective anti-Markovnikov addition of thiols to vinyl ethers upon mild heating, without the need for solvents or catalysts. To elucidate the high selectivity for forming the anti-Markovnikov product, they suggested a mechanism (Figure S10A, Supporting Information). Here, the thiol acts as a hydrogen bond donor,[41] and the oxygen of the vinyl serves as a hydrogen bond acceptor, further activating the thiol and the vinyl. This interaction guides the double bond through a 5-membered intermediate, ultimately yielding only the anti-Markovnikov product. Our findings corroborate this mechanism as with increasing amounts of DBU, the thiol loses its acidic hydrogen, thereby first inhibiting (1 mol%) and further suppressing (10 mol%) the

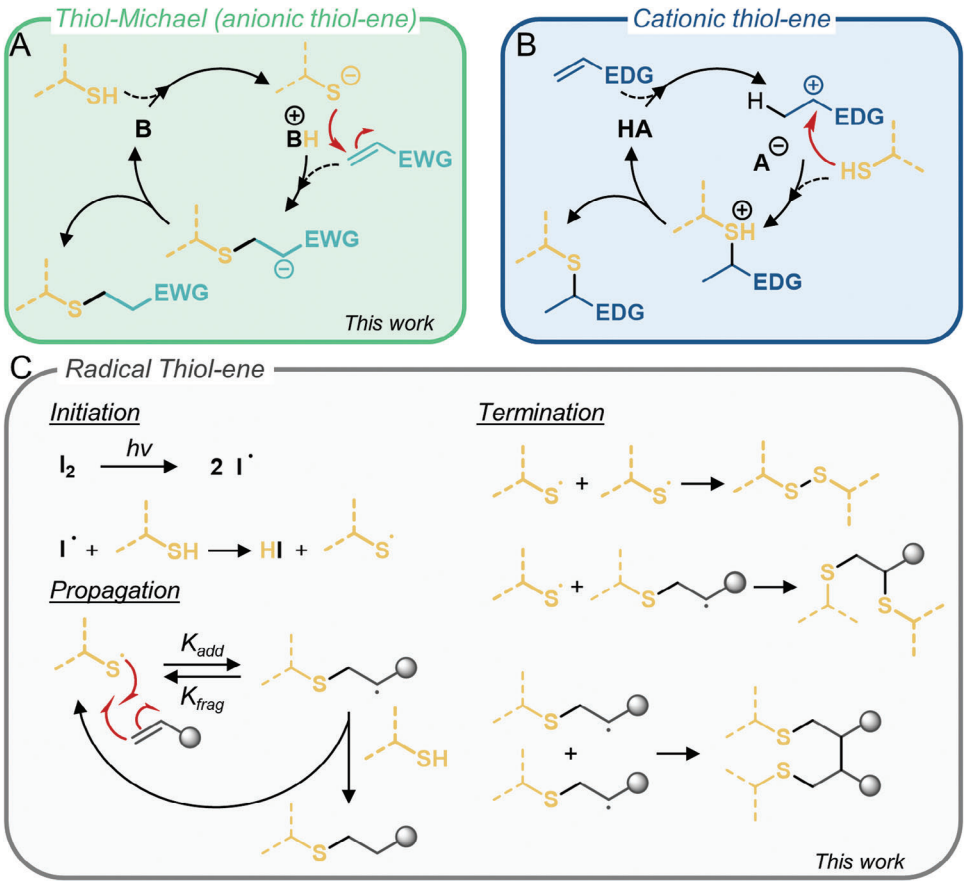

Scheme 1. Simplified mechanisms of A) anionic thiol-ene (thiol-Michael addition), B) cationic thiol-ene, and C) radical thiol-ene (thiol-ene) reactions. EWG stands for electron withdrawing group while EDG for electron donating group.

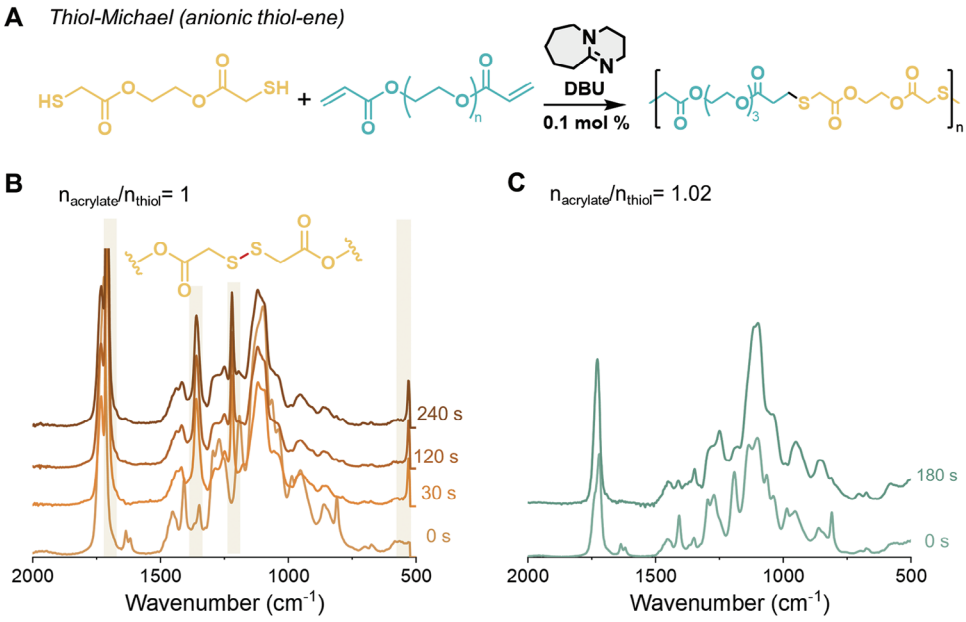

Figure 2. A) thiol-Michael addition reaction between a diacrylate and a dimercaptoacetate. B) FTIR spectra of an equimolar mixture of PEGda and GDMA (highlighted in brown characteristic disulfide bands), and C) the same mixture but with 2mol% excess of diacrylate, taken at different reaction times after 0.1mol% DBU addition.

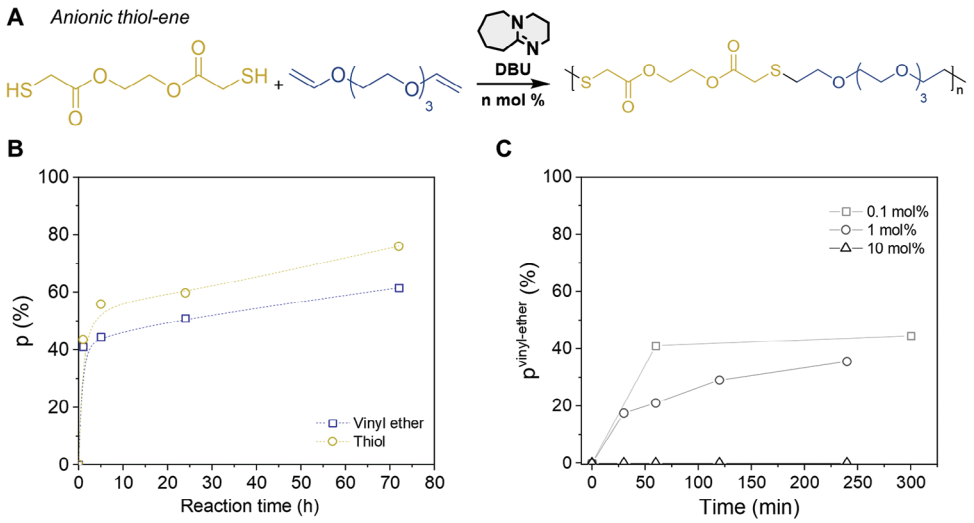

Figure 3. A) Thiol-Michael addition reaction between GDMA and TEGdv, and; Conversion of thiols and vinyl ethers calculated from ^{1}H NMR spectra of aliquots taken at different reaction times, for the B) Thiol-Michael addition reaction between GDMA and TEGdv with 0.1mol% DBU in respect to thiols over a period of 72 h, and of the C) same reaction conducted with distinct DBU concentrations.

reaction. However, the fact that the reaction does not happen at room temperature under uncatalyzed conditions indicates that in the case of the mercaptoacetate reaction with vinyl ethers, the formation of a cyclic intermediate that guides the uncatalyzed anti-Markovnikov addition (Figure S10B, Supporting Information) may not occur. Instead, it is triggered by low amounts of base (0.1 mol% DBU), suggesting that the H-bond activated double bond undergoes an anti-Markovnikov attack of a thiolate (Figure S10B, Supporting Information). In this case, the regioselectivity is given by the thiolate large volume, which guides toward the less sterically hindered anti-Markovnikov position, which is also more electron deficient due to the H-bonding of the ethereal oxygen.

Furthermore, we have verified that vinyl ethers react fully with thiols upon radical initiation, as the conversion of thiols with respect to vinyl is nearly equal, Figures 3B and S3B–I. Furthermore, no peaks related to aliphatic backbones originated from vinyl ethers homopolymerization, or peaks associated with disulfides are observed in the ^{1}H NMR spectra of the radical-catalyzed reaction between TEGdv (1.02 equiv.) and GDMA (Figure S3B–II) which highlights the selectivity of radical thiol-ene polymerization of thiols and vinyl ethers.

Considering this reaction, and as one of the key aspects of our strategy is to be able to perform the thiol-acrylate base-catalyzed reaction in the presence of vinyl ethers, we performed a model reaction with equimolar quantities of GDMA (1 equiv.), triethylene glycol diacrylate (TEGda, 1 equiv.) and TEGdv (1 equiv.) (Figure S11, Supporting Information) catalyzed by 0.1 mol% of DBU. In such conditions it was verified that the thiol-acrylate reaction also occurs rapidly ($t < 15$ min) when in the presence of vinyl ethers, Figure S11 (Supporting Information), while vinyl ethers remain unreacted, confirming the thiol-acrylate/vinyl ether orthogonality upon base-catalysis. However, it is clear that if there is any free thiol in the presence of excess free vinyl ether groups, they will react in the presence of low DBU concentrations to form thioether bonds.

Therefore we envision that if: I- a first step is carried, consisting of the reaction between thiols, acrylates, and vinyl ethers, with excess of thiols in respect to acrylates, and excess of vinyl-ethers in respect to thiols to avoid disulfide formation, by anionic thiol-ene polymerization, and; II- a second step consisting of the addition of a tri-thiol crosslinker to react with the remanent vinyl-ether groups together with a radical photoinitiator, will allow a perfectly defined, side-reaction free, network.

2.2. Exploiting the Orthogonal Reactivity to Prepare Well-Defined Cross-Linked Structures and Its Comparison with FRP-Based Photocured Networks

In order to evaluate the benefit of the sequential thiol-Michael/-ene polymerizations to produce better-defined chemically crosslinked networks, when compared to the traditional acrylate-thiol radical thiol-ene approach, we prepared 3 different networks whose composition in terms of functional groups and backbone structure are shown in **Figure 4**.

To compare our approach we have formulated three different formulations. The first network (thiol-ene/FRP) comprises both thioether bonds and aliphatic acrylic backbones derived from FRP (Figure 4A), while the second network (thiol-Michael/FRP) has the same chemical structure, but FRP happens only in the second step (Figure 4B). In the second case, however, the thiol-Michael addition first step leads to a pre-polymer structure that may favor a better-defined microphase behavior when compared to the first thiol-ene/FRP network, in which both polymerizations are carried simultaneously. Finally, the third network prepared through our proposed strategy (thiol-Michael/ene) contains only thioether bonds that are formed on the sequential polymerizations (Figure 4C).

All networks are formulated using diacrylate functional pre-polymer (CN) which is based on poly(propylene glycol) (PPG) (Figures S12 and S13, Supporting Information). The pre-polymer

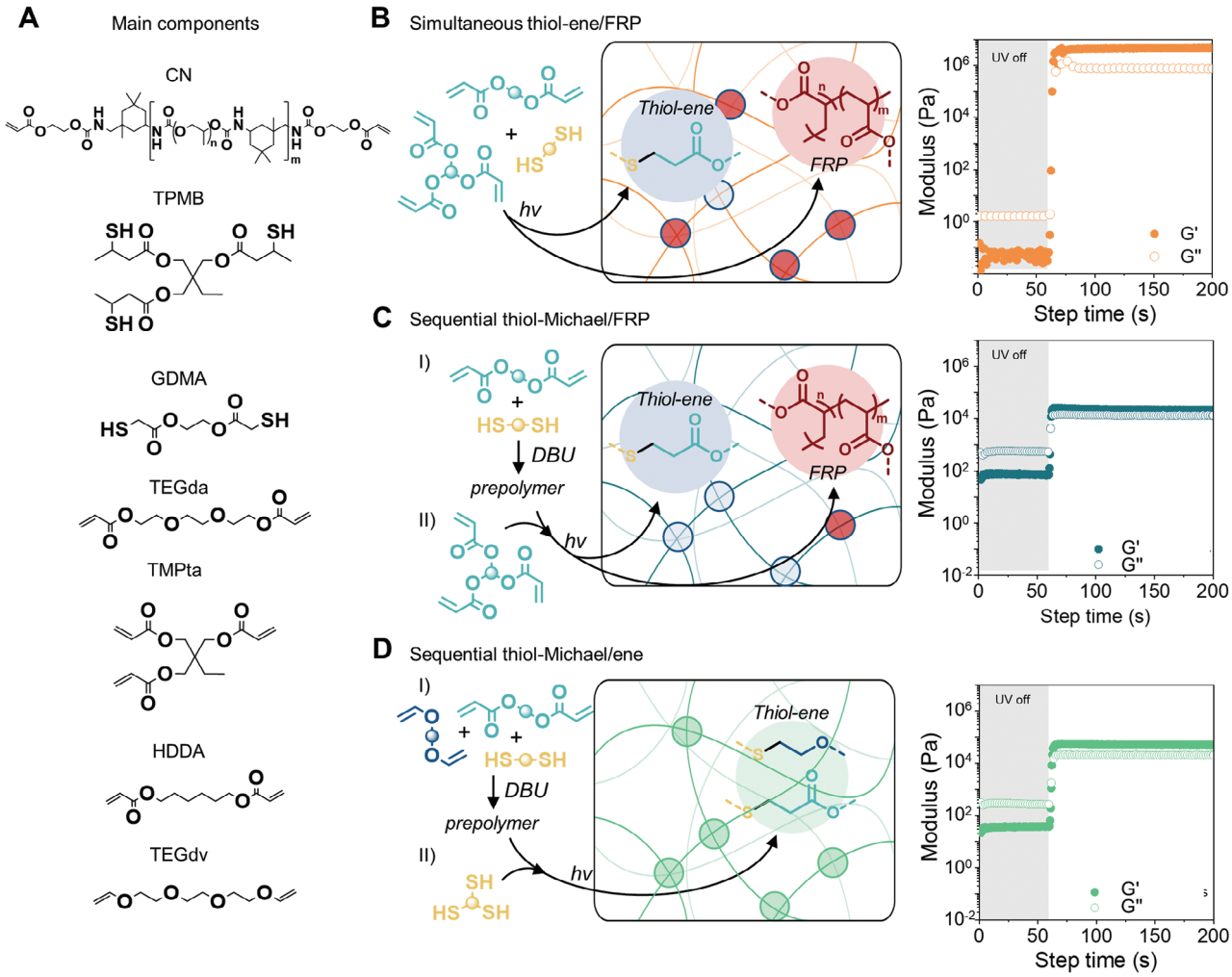

Figure 4. A) Chemical structure of the major components of the formulation. Synthetic procedure and schematic representation of the three networks, with the photorheology data showing the intercrossing of the storage (filled dots) and loss (empty dots) moduli after UV-irradiation, being B) thiol-ene/FRP, C) thiol-Michael/FRP, and D) thiol-Michael/ene, characterized by distinct chemical bonds present on the linear connections and crosslinking points.

has high viscosity, therefore, to allow lower viscosity homogeneous mixtures, hexanediol-diacrylate (HDda) is used as a diacrylate diluent. The composition of the three networks is almost equal, as GDMA, HDda, and TEGdv, were used in all cases in similar concentrations. The difference is found solely in the functionality of the tri(ethylene-glycol) moiety, being a diacrylate for the thiol-Michael/FRP (Figure 4C), and a di(vinyl ether) for the sequential thiol-Michael/ene formulations (Figure 4D). The detailed composition of the three formulations is presented in Table S1 (Supporting Information).

After irradiating the formulations to UV light (10 mW cm^{-2}) for 2 min they presented gel content >85% after the curing step, Figure S14 (Supporting Information), attesting to an effective network formation regardless of the polymerization mechanism explored. The photocuring of all the formulations was confirmed by photorheology experiments showing the intercrossing of storage, and loss moduli, and the higher storage moduli of all the formulations after curing upon a frequency sweep (Figure 4B–D). The higher shelf-life stability for the thiol-Michael/ene formulation is confirmed by practically no change in viscosity over 5 days Figure S15 (Supporting Information). On the other hand, the thiol-Michael/FRP resins had a low shelf-life stability of 1 day, as observed by the substantial increase in its viscosity of one order of magnitude Figure S15 (Supporting Information). This is due to the formation of pre-polymers. Presence of such acrylate end-groups (thiol-Michael/FRP), and vinyl ether end-groups with undetectable unreacted thiols (thiol-Michael/ene), as well as the absence of side reactions in both cases, and chemical structure of the resins after DBU addition, was confirmed by ^{1}H NMR, Figures S16 and S17 (Supporting Information).

Although having analogous compositions, Table S1 (Supporting Information), the distinct network formation mechanisms of the formulations thiol-ene/FRP, thiol-Michael/FRP, and thiol-Michael/ene present substantial differences in the network chemical structure and topology. However, these distinctions do not lead to any expressive differences in the FTIR spectra, Figures S18 and S19 (Supporting Information).

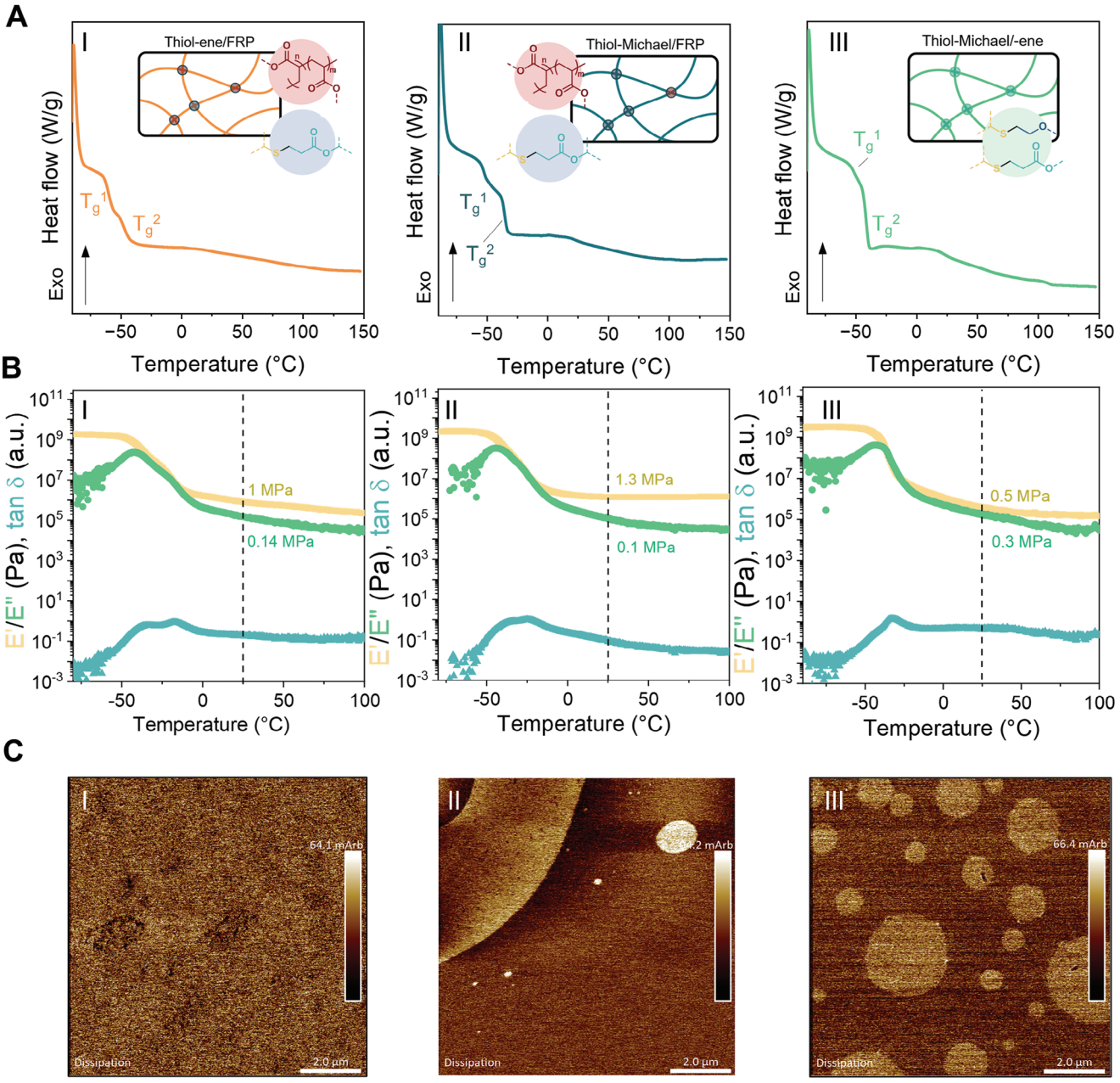

Figure 5. A) 2nd heating DSC curves, B) DMTA curves of storage moduli (E′), loss moduli (E″) and tan δ curves, and C) AFM dissipation mode images of spin-coated cured adhesive films for **I** thiol-ene/FRP, **II** thiol-Michael/FRP, and **III** thiol-Michael/ene cured adhesives.

2.3. Effect of Network Topology on Thermal-Mechanical Properties and Phase-Behavior of PSA Films

The DSC curves presented in **Figure** 5A evidence that in the three adhesive films, there is the presence of two distinct amorphous phases with distinct T_g values. Such heterogeneities can be a consequence of the multi-block nature of the networks, providing covalently connected amorphous nano/micro-domains of distinct composition and thus distinct glass transition temperatures as a result of microphase separation, or even phase separation. Glass transition temperatures obtained from both DSC and dynamical mechanical thermo-analysis (DMTA) are summarized in Table S2 (Supporting Information).

There is a large variety of segments present in the networks obtained using FRP, Figures S20–S22 (Supporting Information), which hinders ordered microphase separation due to the high structural randomness of the multi-block network, despite the relatively high Flory interaction parameter of polyacrylates, polythioethers, and polyethers.[42,43] Both thiol-ene/FRP and thiol-Michael/FRP adhesives contain FRP acrylic chains with distinct pendant groups and length, combined with step-growth polythioether chains with a considerable mass fraction (≈40wt%) of

polyether chains derived from the PPG of the diacrylate functional pre-polymer (Table S1, Supporting Information). It is unlikely that such provides well-defined microphase-separated amorphous phases, while maybe presenting highly undefined microphase separation or even macroscopic phase separation.

It is possible to infer that the lower T_g ≈−50 °C is related to the PPG-richer amorphous phase, by comparison with the DSC of the neat PU-diacrylate CN, Figure S23 (Supporting Information), present in all formulations. On the other hand, the second and higher T_g in between −25 and −40 °C (Figure 5A-I) is probably related to the amorphous phase richer in polythioether and acrylic chains, in the case of the thiol-ene/FRP and thiol-Michael/FRP formulations, and solely polythioether chains for the thiol-Michael/ene formulations. This hypothesis is supported by the fact that HDda polyacrylate (pAc) has a T_g ≈0 °C, similar to the one of methyl polyacrylate,[44] and higher than the T_g found for the polythioether homopolymers of −40 °C (Figure S23, Supporting Information). Such results explain the highest second T_g of −18 °C for the thiol-ene/FRP formulation, which has the highest volume fraction of acrylic chains, and so its polythioether/acrylate phase has higher T_g.

The thiol-Michael/FRP formulation (Figure 5A-II), on the other hand, which also presents polyacrylic chains, although likely in less quantity and of lower molar mass when compared to thiol-ene/FRP, has an intermediate 2nd T_g of −23 °C. Finally, the thiol-Michael/ene formulation (Figure 5A-III), which second T_g relates to a "pure" polythioether amorphous phase, which does not contain acrylic chains, has the lowest second T_g of −33 °C. Such value for the second T_g (−33 °C) is slightly higher than those of the pure polythioethers (poly(GDMA+TEGdv)), Figure S23 (Supporting Information), produced by radical thiol-ene, and poly(HDda+GDMA)) synthesized by anionic thiol-ene, probably due to the lower mobility provided by the chemical crosslinking.

The absence of FRP in the thiol-Michael/ene formulation also promotes a lower crosslinking expressed by the lowest difference between storage and loss moduli (ΔE) within all the formulations of 0.2 MPa, in contrast with 1.2 MPa (thiol-Michael/FRP), and 0.8 MPa (thiol-ene/FRP), as verified by DMTA (Figure 5B).[45,46] The lower degree of crosslinking of thiol-Michael/ene formulation together to a potentially better-defined microphase separation may contribute to its adhesive properties. The distinct α-transitions are also verified by DMTA, Figure 5B, appearing as peaks/shoulders in the Tan α and loss moduli curves.[45]

Figure S24 (Supporting Information) shows pictures of the adhesive formulations prior to the addition of DBU, for the thiol-Michael addition-containing formulations, and before photocuring for the simultaneous thiol-ene/FRP. Homogeneity is confirmed by a single T_g in the first heating scans for all the formulations (Figure S25, Supporting Information). After the addition of DBU, formulations thiol-Michael/ene and thiol-Michael/FRP undergo thiol-Michael addition polymerization and turn opaque (Figure S24, Supporting Information). We hypothesize that this occurs on thiol-Michael/ene due to liquid-liquid phase separation into a PPG-rich disperse phase which scatters light, and a polythioether-rich continuous phase, with some di(vinyl ethers) remaining as diluent. On the other hand, in the case of thiol-Michael/FRP, we hypothesize that the opacity after DBU addition is a result of a poorly defined phase separation that occurs in the liquid state, upon the formation of domains of distinct composition, PPG-rich and polythioether rich, driven by the random multiblock nature of thiol-Michael/FRP after thiol-Michael addition step.

Such hypothesis is supported by DSC measurements which show two T_g's for both formulations after DBU addition, Figure S26 (Supporting Information), and by oscillatory rheometry (Figure S27, Supporting Information) which shows a pseudoplastic behavior typical of liquid–liquid phase-separated resins. After UV irradiation which leads to thiol-ene polymerization for thiol-Michael/ene, promoting crosslinking, the cured solid polymeric film increases in transparency, making it possible to address it visually, Figure S24 (Supporting Information).

Figure 5C shows images of AFM acquired in the dissipation mode that were used to address the phase behavior of the adhesive network surfaces at 25 °C. The thiol-Michael/ene network possesses a well-defined phase-separated morphology with two distinct amorphous phases, one dispersed globular phase (clearer) of distinct mechanical response with respect to the continuous phase (darker), Figure 5C. As verified on the topography images, Figure S28A (Supporting Information), the region observed is flat for the thiol-Michael/ene network, with a height difference of ≈10 nm, therefore, the contrast verified on the dissipation images are related to composition differences within the phases that yield distinct mechanical response. This is a consequence of the liquid-liquid phase separation that occurs in the thiol-Michael addition step, which forms PPG-rich globules within the polythiother-rich continuous phase. Since the soft polyether PPG segments are present in a lower mass fraction, and so volume fraction, in the thiol-Michael/ene formulation, it is reasonable to infer that the clearer spherical phase is related to the PPG-richer amorphous phase. This is also supported by the fact that in the dissipation mode of AFM, clearer domains are related to softer phases.[47,48] On the other hand, the continuous, darker, and more rigid phase is related to the polythioether segments composed of HDda, TEGdv, and GDMA, which have a higher T_g of −33 °C with respect to the PPG-rich amorphous phase, of −48 °C Figure 5C. The spherical domains have an average diameter of 1.0 ± 0.8 µm, as determined by AFM upon the diameter measurement of over 50 globules.

The network thiol-Michael/FRP also presents clearer spherical domains dispersed into a continuous darker phase, and analogously to thiol-Michael/ene, the regions observed are flat with a height variation of ≈10 nm (Figure S28B, Supporting Information). However, the dispersed globular domains are much smaller and scarce, in comparison with the phase-separated morphology found for the thiol-Michael/ene network. This can be due to the lower definition in terms of the block-like architecture of the thiol-Michael/FRP formulation, in comparison with the thiol-Michael/ene, being already a long-chain random multiblock copolymer after the thiol-Michael addition step, with no residual low-molar mass plasticizers (Figure S30, Supporting Information). Such contributes to the increase in miscibility, thus decreasing in size and number of the domains. In addition, considering that the PPG-rich globules have higher polarity, it is likely that such phase is present on the surface to a smaller extent, contributing to the lower number of such globules, in comparison to the thiol-Michael/ene formulation.

At last, there are no distinct phases on the dissipation images acquired for the thiol-ene/FRP network, Figure 5C-I being the

darker regions observed in the image associated with the surface roughness, which in this case is high on the order of 60 nm (Figure S28C, Supporting Information). When dissipation images are acquired with higher magnification, no distinct domains are observed for the thiol-ene/FRP formulation. Such can be due to a lower degree of phase separation in the microscopic range, resulting from a poorly defined block structure provided by simultaneous thiol-ene/FRP polymerizations. However, the thiol-ene/FRP presents macroscopic heterogeneities that can be visually addressed as more transparent and white regions (Figure S29, Supporting Information). Therefore, it is clear that some phase separation is occurring and is the origin of the two distinct glass transitions observed by DSC and DMTA, but each phase itself has a low degree of microphase separation, compared to the other two compositions. This associated with the possible difference between surface and bulk compositions, explains the absence of phase-separation in the AFM images, as it is related to the surface of the thiol-ene/FRP network, thus, not allowing visualization of possible microscopic phases present in the bulk.

The increase in transparency upon photo-curing of thiol-Michael/ene, Figure S24 (Supporting Information), is likely related to the polymerization-induced shrinking of the disperse phase, associated with a reduction in the refractive index difference (Δn) promoted by the presence of polythioether in both phases after photocuring.[49,50] Prior to thiol-ene, the PPG-rich disperse phase of thiol-Michael/ene is poor in thioether bonds, after the photocuring of the TEGdv, GDMA and the tri-thiol crosslinker that is present in both disperse and continuous phases react forming thioether bonds, crosslinking the system, and reducing both sizes of the dispersed phase and Δn, decreasing substantially the light scattering intensity. Such phenomena do not occur on thiol-Michael/FRP formulation, which remains opaque after FRP photocuring, probably because Δn is further increased by the formation of polyacrylate chains, which have distinct refractive index than polyether and polythioether. On the other hand, thiol-ene/FRP formulation is also opaque after simultaneous thiol-ene/FRP photocuring, which may be related to the competing polymerization mechanisms. While FRP is a chain-growth polymerization, forming high molar mass chains at low conversion values, thiol-ene polymerization is step-growth, thus only forming high molar mass chains at high-conversion values. Therefore, it is likely that the thiol-ene/FRP undergoes phase separation between a polyacrylate-rich amorphous phase that solidifies priorly to the polythioether/PPG-rich amorphous phase, forming distinct macroscopic phases that can be addressed visually, Figure S29 (Supporting Information).

2.4. Mechanism Proposal for Micro-, and Nanophase Separation

Scheme 2 presents a schematical representation of the liquid-liquid phase separation process followed by crosslinking undergone by the thiol-Michael/ene formulation. Initially, a homogeneous mixture of small molecules (diacrylate diluent, di(vinyl ether), dithiol) with the PPG-based diacrylate pre-polymer is found (Scheme 2A). Upon addition of DBU, several polymerization reactions increase the size of the molecules, which reduces the contribution of the entropy of mixing and drives the system to a liquid-liquid phase separation process (Scheme 2B). Such polymerizations are: 1) The extension of the PPG-based diacrylate with dithiol forms longer-chain polyether copolymers comprising thioether bonds between the diacrylate and dithiols as a chain-extending unit, 2) the formation of polythioether oligomers consisted of the reaction between the diacrylate diluent and the di(vinyl ether) with the dithiol, 3) copolymerization of such polythioether oligomers and the longer-chain polyether copolymers.

The colloidal stability of such liquid-liquid phase separated system is promoted by the sterical hindrance provided by the presence of the PPG-oligomeric thioether copolymers, which stays at the interface of the PPG-rich disperse globular phase with the continuous polythioether phase. Such suppresses both macroscopic phase separation and globular aggregation (Scheme 2B), as confirmed by the negligible increase in viscosity of the mixture after 5 days of DBU addition (Figure S15, Supporting Information). At last, the globular phase-separated morphology is finally fixed via the chemical crosslinking of the system via radical thiol-ene (Scheme 2C), which leads to a shrinkage of the globular phase, and an increase in the density of thioether bonds in both dispersed and continuous phases, also reducing the Δn between the phases. Both combined increase the transparency of the adhesive film, Scheme 2C, by drastically reducing the scattering intensity.[49,50]

In addition to the liquid-liquid phase separation, which promotes a well-defined globular phase-separated morphology, the thiol-Michael/ene networks also comprise nanophases as a result of a thermodynamically driven nanophase-separation process undergone by the multi-block network inside the globular phase. As previously mentioned, the PPG-rich globular phase also contains polyurethane linkages and short-chain polythioether blocks. The PU bonds are formed by the reaction between the hydroxyethyl acrylate and the isophorone diisocyanate terminations of the PPG pre-polymer (Figure S12, Supporting Information), providing the acrylate-terminated PU-prepolymer based on PPG and IPDI (CN). On the other hand, the thioether blocks are formed in the thiol-Michael addition step, between such acrylate terminations, the dithiol (GDMA), and the diacrylate diluent (HDda). The covalent interconnection between such blocks of relatively high Flory interaction parameters leads to a nanophase separation process, often referred to as self-assembly.[51] This process is driven by the reduction in the Gibbs free energy of mixing, upon reducing the interfacial area between the blocks of low chemical affinity which happens by the formation of two distinct micro/nanophases, each rich in one of the blocks. In this situation, the interfacial area between the blocks is minimized and consists of the interface between the micro/nanophases, and the macroscopic phase separation is impossible because the blocks are connected covalently.

The microphase-separated morphology of the thiol-Michael/ene network could be verified by exaggerating the contrast on the AFM images, **Figure 6A**, in which it is clear that the globular phase contains nano-domains. Besides, such nanophases can be better addressed visually in the TEM images in Figure 6A, as due to the polyether's higher oxygen density, the phases richer in PPG are darker due to a higher density of Ru tetroxide-oxygen complexation. The images clearly show clearer phases in between darker phases for the PPG-rich globular phase, due to the microphase separation between

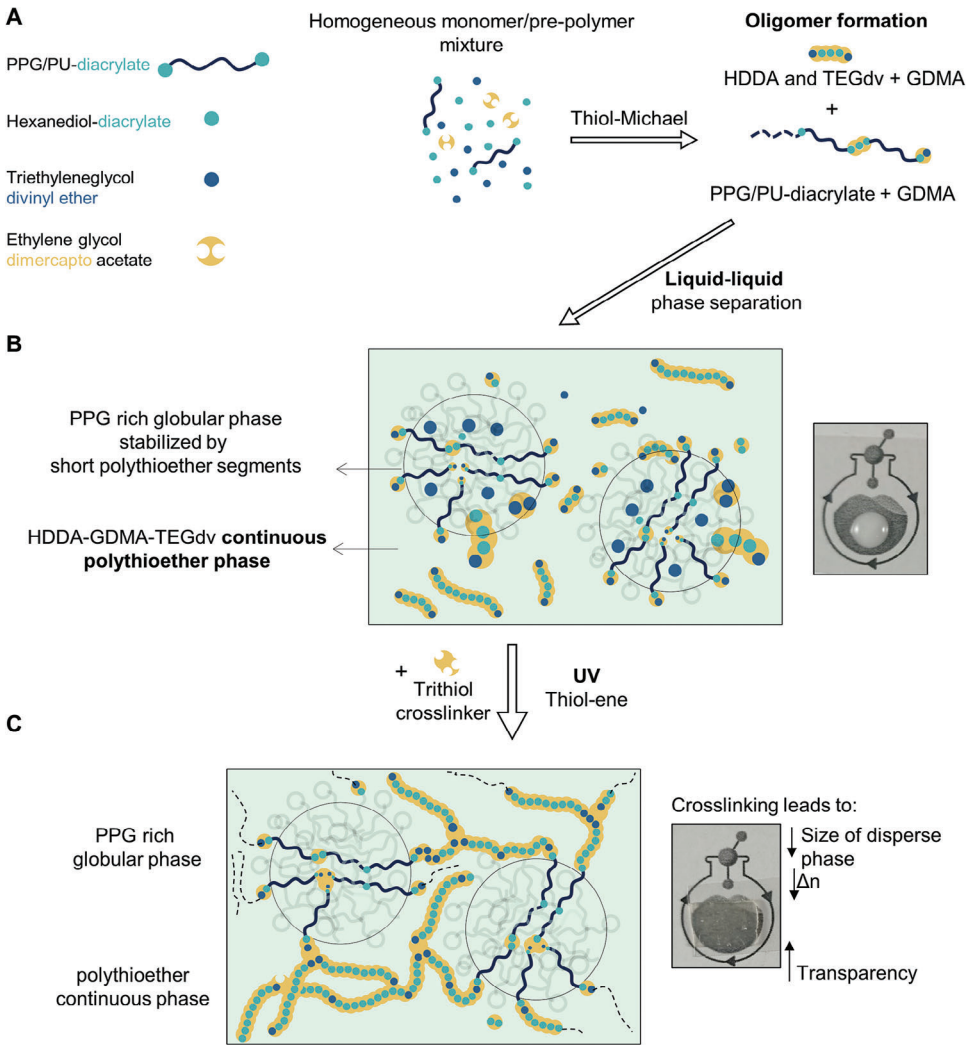

Scheme 2. Liquid–liquid phase separation process underwent by thiol-Michael/ene adhesive formulation after: A) thiol-Michael addition polymerization which forms polythioether oligomers formed by the thiol-Michael addition reactions of the dithiol with divinyl ether and diacrylate small molecules, and with PPG/PU-diacrylate, which drives a B) liquid–liquid phase separation process that is followed by C) photocuring via radical thiol-ene, which sustains the phase separated morphology into a chemically crosslinked matrix.

the PPG blocks, and the short-polythioether blocks formed in both thiol-Michael addition and thiol-ene steps, Figure 6A,B. It's clear that the length of interdomain interspacing between darker and clearer phases found in the PPG-rich globular phase, corresponding to the polythioether-rich, and PPG-rich phases, respectively, falls within the nanoscopic range, 10–100 nm. At last, small-angle X-ray scattering (SAXS) experiments were carried out to confirm the presence, or not, of a nanophase-separated morphology in the thiol-Michael/ene network, Figure 6C, and to allow a quantitative description of the phase behavior in the nanoscale.

As verified in the SAXS plots, Figure 6C, all the networks show inflections in the X-ray scattering profile that indicate the presence of phase separation with domain-spacing (l) in the nanoscale (1 nm < l < 100 nm). However, the absence of a clear peak in the case of the thiol-Michael/FRP and thiol-ene/FRP networks, confirmed by the plots of the derivative of the scattering intensity with respect to the scattering vector (q), which shows no intersection with the x-axis, suggests that such phase-separation is highly disordered in the case of both networks. In contrast, our thiol-Michael/ene formulation presents a maximum in the SAXS plot, Figure 6C, confirming the higher ordering and the narrower distribution of domain-interspacing of its nanophase-separated morphology,[52–56] when compared to its compositional analogs obtained by distinct polymerization mechanisms. By taking the value of q of the peak-maxima, it is possible to calculate the correlation distance ($d = 2\pi/q$), which gives the average distance between the center of each dispersed nanophase present in the sample.[50,57] The correlation distance of 27.0 nm was determined for the thiol-Michael/ene network, Figure 6C, and is similar to the estimated length of the soft-block of PPG-IPDI, present in the PU-diacrylate pre-polymer, Figure 6B. The length of the PPG-based soft block was estimated using the average length of the poly(ethylene glycol) monomeric unit,[58] which analogously to PPG, comprises two carbons and one oxygen in the backbone of the monomeric unit.

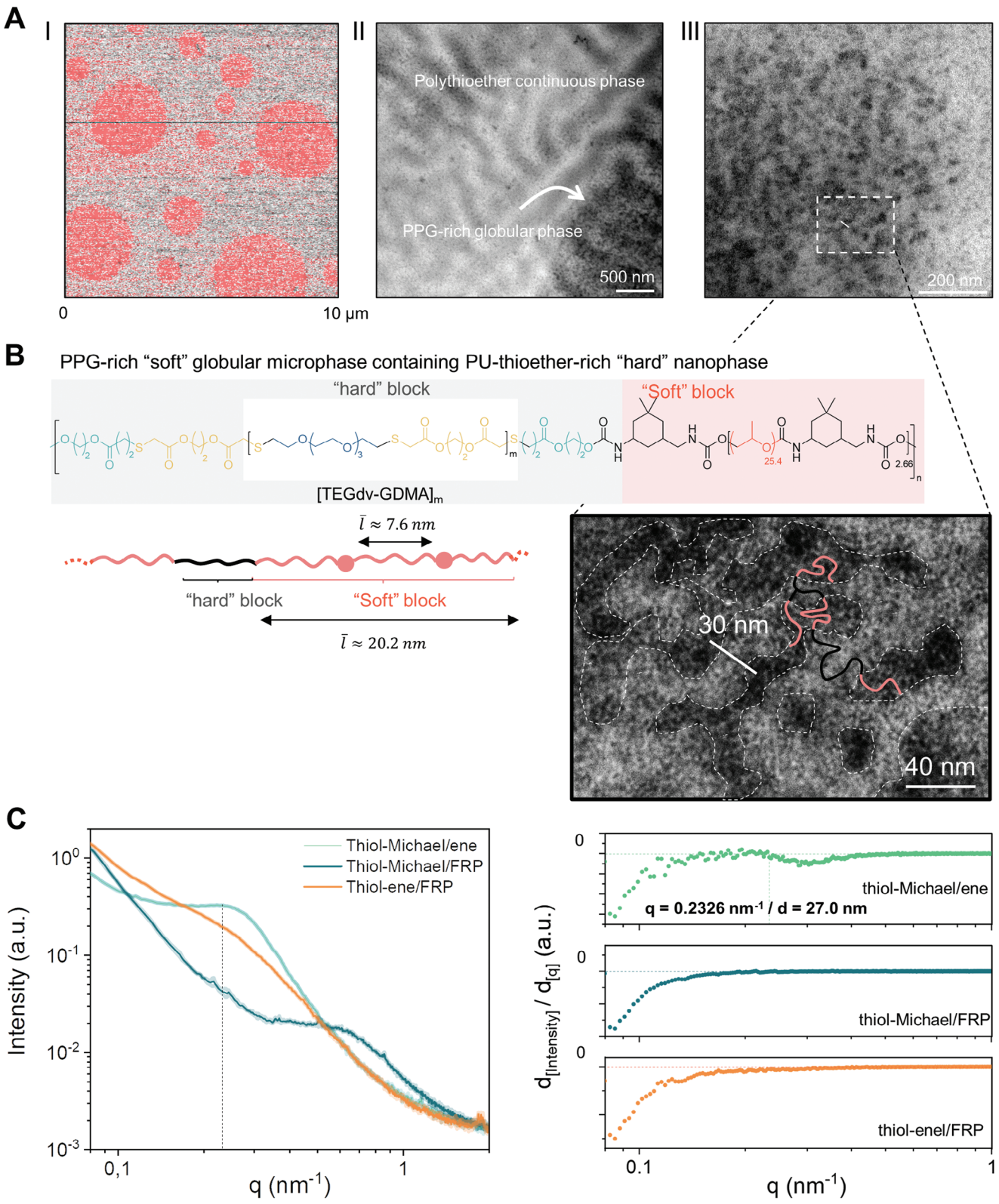

Figure 6. A) AFM image with enhanced contrast, and Ru-stained TEM images of cryo-microtonated cross-sections of the thiol-Michael/ene network. B) Scheme of the microphase separated morphology of the PPG-rich globular phase happening in the thiol-Michael/ene network. The scheme shows a magnified region of the TEM image with darker regions highlighted by a white dashed line, and each block of the macromolecule occupying the phase in which they are in higher concentration. C) X-ray scattering intensity versus q (Ieft), and derivative of the scattering intensity versus q (right) obtained by SAXS for the three distinct networks.

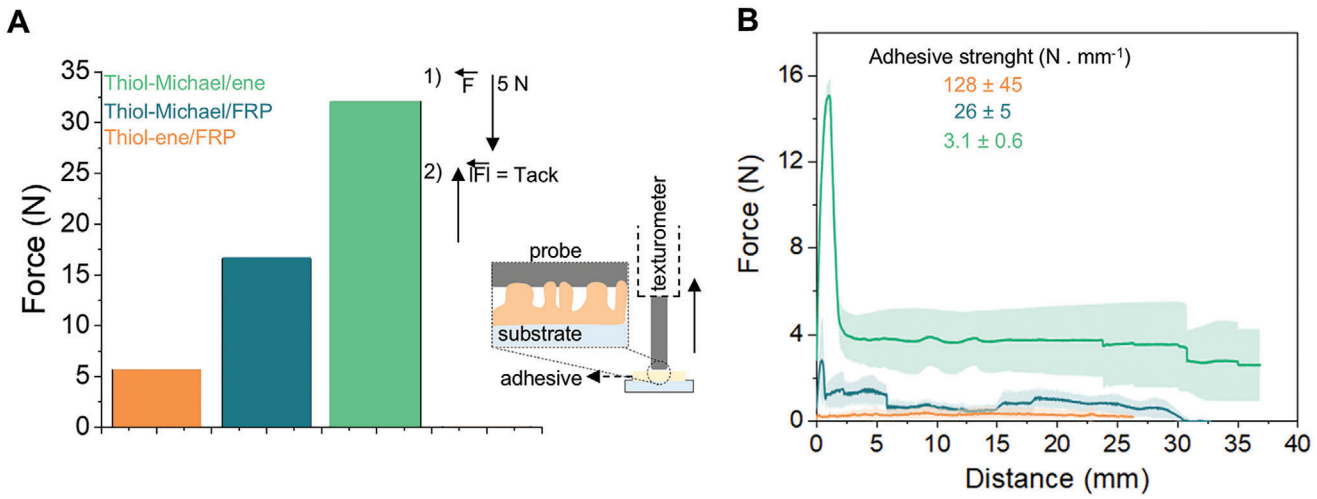

Figure 7. Plots of A) Tackiness, and B) peeling trials for the distinct adhesive formulations. A schematic representation of the tackiness trial is shown in Figure (A).

As the nanophase-separation process undergone by block-copolymers is a thermodynamically driven process in which each of the nanophases is majorly composed by one of the blocks of distinct chemical structure, both domain-size and spacing needs to be in the range of the length of the blocks of the copolymer.[51] This is true for the thiol-Michael/ene network, as shown in Figure 6B, the estimated length of the PPG-based soft block is on average 20 nm, and that of the PU-thioether hard block should be necessarily smaller given the lack of equimolarity between thiols and vinyls in the thiol-Michael addition step, which yields low-molar mass blocks due to the step-growth nature of such polymerization. Therefore, the results of SAXS agree with a nanophase-separated morphology derived from the segregation of covalently connected PPG-PU blocks and PU-thioether blocks present in the PPG-rich globular phase. Such is only present in the thiol-Michael/ene formulation due to its better block-like definition provided by a pure step-growth polymerization crosslinking mechanism, with negligible side reactions.

2.5. Effect of Network Chemical Structure and Composition on Pressure-Sensitive Adhesive (PSA) Properties

As previously mentioned, the peeling strength and tackiness, key properties for pressure-sensitive adhesives, are directly related to the crosslinking density, chain length between crosslinking points, and surface homogeneity.[59,60] Longer chain length between crosslinking points eases polymer-surface entanglements, as well as a lower crosslinking density. The distinct chemical crosslinking mechanisms undergone by the three different formulations of analogous compositions investigated directly influence such properties, as discussed in the previous topic, which shall thus influence both adhesive strength and tackiness. To investigate such influence, initial tackiness trials were conducted for the adhesives on metal substrates upon applying 5 N of force for 3 min, **Figure** 7A. The thiol-Michael/ene adhesive has the highest tackiness value of 32 N, while thiol-Michael/FRP has an intermediate value of 16 N, and thiol-ene/FRP has the lowest tackiness value of 5 N. Being the three formulations of similar composition, such difference in tackiness value can only be related to the descending order of crosslinking density of the thiol-ene/FRP, thiol-Michael/FRP, and thiol-Michael/ene formulations, and the improved network topology of the thiol-Michael/ene formulation. While thiol-Michael/ene reduced crosslinking is provided by the "pure" step-growth crosslinking motif, for the thiol-Michael/FRP the sequential FRP step underwent after thiol-Michael addition provided longer segments of polythioether that are unlikely to be produced on the simultaneous thiol-ene/FRP reaction. Such simultaneous distinct polymerization mechanisms provide macroscopic heterogeneities, as previously discussed, a higher crosslinking density due to two competing crosslinking mechanisms, and uncontrolled number of chains linked by crosslinking points, all of which explain thiol-ene/FRP lowest tackiness value.

To address the three distinct formulations of adhesive strength, peeling trials were conducted on metal substrates upon the application of 5 N of force for 3 min to the substrate-adhesive test probe, Figure 7B. The thiol-Michael/ene formulation drastically outperforms the other two formulations with a peeling strength of 0.74 N mm^{-1}, in comparison with 0.2 N mm^{-1} for Thiol-Michael/FRP, and 0.06 N mm^{-1} for thiol-ene/FRP. The peeling strength is also highly related to the network's crosslinking density, chain length between crosslinking points, and homogeneity.[8] All of those improved features are provided by the single step-growth polymerization mechanism of the sequential thiol-Michael/ene strategy.

In addition to that, the sequential thiol-Michael/ene strategy also provides dynamic covalent networks due to a base-catalyzed temperature-triggered dissociative exchange mechanism (Figure 8A).[27] Such features can be explored for improving PSA adhesive strength upon thermal annealing as well as to drastically reduce adhesive strength at high temperatures due to the softening of the adhesive, easing its removal at high temperatures.

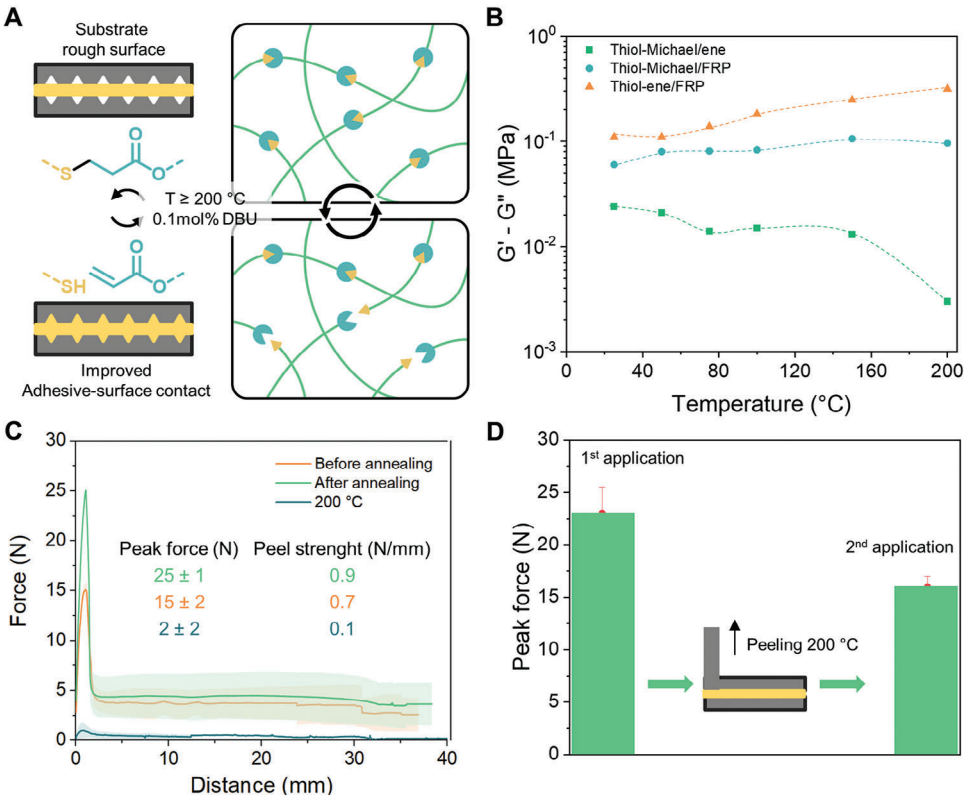

Figure 8. A) Scheme of thermo-switchable behavior and its role on adhesion enhancement upon annealing, B) difference between storage moduli (G′) and loss moduli (G″) at 1 Hz obtained by oscillatory rheometry at distinct temperatures. Peeling plots and adhesive strength values were obtained by peeling trials conducted prior to annealing at 200 °C for 5 min, after annealing at 200 °C for 5 min, and at 200 °C for C) thiol-Michael/ene.

2.6. Exploiting the Dynamic Behavior of the Thiol-Michael Addition to Prepare Switchable Adhesives

The covalent dynamic nature of the thiol-Michael addition containing adhesive formulations was addressed by oscillatory rheometry, **Figure** 8B. The difference between the storage moduli (G′) and loss moduli (G″) drops a whole order of magnitude from 4×10^{-2} MPa to 4×10^{-3} MPa upon heating. In contrast, such difference between storage and loss moduli increases slightly for the other two formulations Figure 8B. This confirms the significant softening of the thiol-Michael/ene adhesive at 200 °C, provided by the temperature-triggered covalent dynamic nature of the thiol-acrylate bonds upon base-catalysis. As such bonds are less present in the other two networks, associated with the presence of permanently crosslinked segments formed via acrylate FRP, the thermal-induced softening does not occur.

As verified on the peeling curves of the thiol-Michael/ene adhesive taken at room temperature before, and after a thermal annealing at 200 °C for 5 min, Figure 8C, the peeling strength is increased from 0.7 to 0.9 N mm^{-1} with thermal annealing. This expressive increase is due to the dynamic behavior of the thiol-Michael/ene network verified by oscillatory rheometry and in agreement with previously reported base-catalyzed thiol-acrylate covalent adaptable networks for other applications.[28]

On the other hand, to achieve reversible on-demand adhesives, either the adhesion or the cohesion of the polymer network needs to be triggered and disrupted to allow the detachment of the surfaces without damaging their substrates.[1] In the past decade, with special attention over the past 5 years, great advancements were achieved in providing stimuli-responsive adhesives that can attach/detach reversibly and upon different stimuli.[61–66] However, the development of low-cost scalable switchable adhesives is highly desirable although still challenging. Moreover, those adhesives must fulfill the industrial requirements and cure in a short period of time.

To address the thermal-switchability of the thiol-Michael/ene adhesive, peeling trials were performed at high temperatures upon heating the substrate-adhesive probe at 200 °C during the trial. Peeling strength reduces to 0.1 N mm^{-1} upon heating at 200 °C, Figure 8C. This confirms the thermo-switchable character of the thiol-Michael/ene pressure-sensitive adhesive. Moreover, the adhesives could be re-applied, with a small reduction in peeling peak force (Figure 8D).

2.7. Lamination Process and Comparison to Conventional Acrylate Chemistry

Finally, the thiol-Michael/ene formulation was produced in a multi-gram scale batch (>20 g) and laminated using an industrial plant. As previously discussed, only thiol-Michael/ene formulation has a high shelf-life stability post-DBU addition. Besides, such a lamination technique could be performed without the N_2 protection layer (**Figure 9**), required for FRP PSA manufacturing,

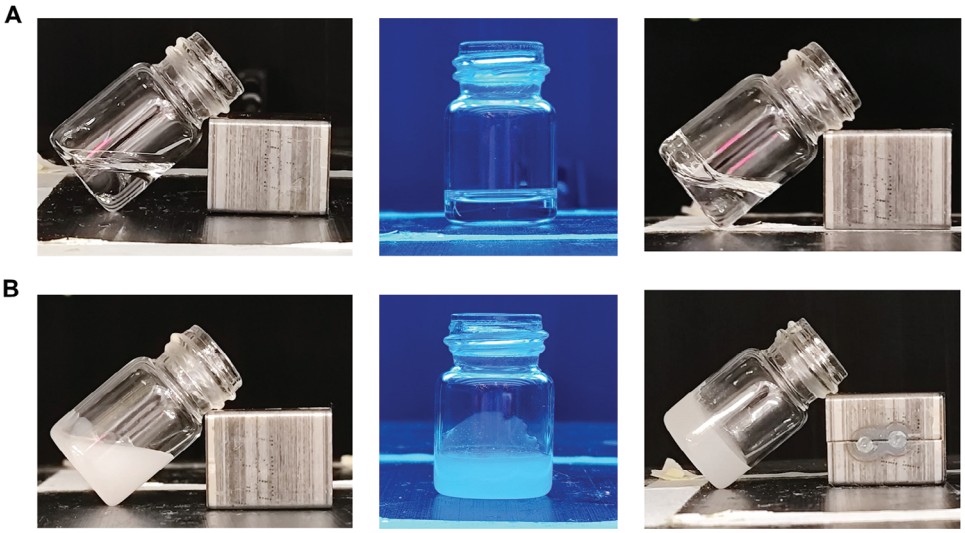

Figure 9. Pictures taken before, during, and after UV-irradiation ($\lambda = 365$ nm) for A) typical acrylic resin used for pressure-sensitive adhesives, and for B) thiol-Michael/ene adhesive formulation.

reducing production costs. As shown in Figure 9, typical free-radical polymerization-based pressure-sensitive adhesive formulations do not cure in normal atmospheric conditions, in contrast with our thiol-Michael/ene-based process. With the reduced cost and increased feasibility of not requiring a protective N_2 layer, our thiol-Michael/ene strategy establishes itself as a strong candidate for the actual production of new high-performance thermo-switchable adhesives for commercial purposes.

3. Conclusion and Outlook

There are several reports regarding materials manufacturing using thiol-ene chemistry, many times with the strong statement that such chemistries are "click-like" under uncontrolled conditions, which is not precise due to the high incidence of side reactions. In this article, it is elucidated the base-triggered room temperature thiol-Michael addition reaction between vinyl ethers and thiols. This fact enables the employment thiol-ene chemistries with high spatial and temporal control by addressing the suppression of thiol and vinyl side reactions, typically undergone in such systems. We demonstrate that vinyl ethers reaction is slower than that of the acrylates with mercaptoacetates upon DBU catalysis and reaches a steady plateau ≈50% conversion with 5 h of reaction, while acrylate-thiol reaches full conversion within 30 s. The negative effect of increasing DBU concentration on the kinetics of such a reaction led to a proposed mechanism in which thiol-vinyl ether H-bond complexes play a key role.

We found that the thiol-Michael/-ene strategy provided the lowest crosslinking density, highest chain length between crosslinking points, and better-defined micro-, and nanophase separation. Such a network comprises dispersed soft globular domains (1.0 ± 0.8 µm) which also contain an inner nanophase-separated structure, led by PU-thioether/PPG-PU phase segregation. The average domain interspacing could be determined by SAXS and is ≈27.0 nm, in the same range as the estimated block lengths. At last, this globular phase is dispersed within a continuous polythioether phase. We verified that the combination of such properties is highly beneficial for the properties of the pressure-sensitive adhesives. Additionally, taking advantage of the acrylate-thiol dynamic behavior, a thermal-induced softening could be promoted allowing the preparation of switchable adhesives. Finally, the high shelf-life stability of the sequential thiol-Michael/ene formulation allowed its production at a multigram scale, followed by its photocuring using an industrial lamination process without N_2 protective layers, as a token of the adhesive scalability and O_2 insensitivity, in contrast to FRP-based PSAs. Therefore, this study lays the groundwork with thiol-vinyl chemical design and reaction screening, allowing the development of well-defined thiol-Michael/ene networks produced with good temporal and spatial control showing great potential for industrialization and commercial application.

Supporting Information

Supporting Information is available from the Wiley Online Library or from the author.

Acknowledgements

The authors acknowledge grant TED2021-129852B-C22 funded by MCIN/AEI/10.13039/501100011033 and by the European Union NextGenerationEU/PRTR and the grant PID2022-138199NB-I00 funded by MCIN/AEI/10.13039/501100011033. The authors acknowledge grant TED2021-129852B-C22 funded by MCIN/AEI/10.13039/501100011033 and by the European Union NextGenerationEU/PRTR and the grant PID2022-138199NB-I00 funded by MCIN/AEI/10.13039/501100011033. L.P.F. thanks the ADAGIO: Advanced Manufacturing Research Fellowship Programme in the Basque e New Aquitaine Region. The authors would like to thank the financial support provided by the NIPU-EJD project; this project has received funding from the European Union's Horizon 2020 research and innovation program under the Marie Skłodowska-Curie grant agreement No 955700. The authors acknowledge the financial support from the European Union's Horizon 2020 research and innovation program, under the Marie Skłodowska-Curie grant agreement no. 101034379. MX acknowledges the grant from the Gipuzkoa Fellows

Programme (G75067454). SAXS experiments were performed at BL11-NCD-SWEET beamline exp.2023027561 at ALBA Synchrotron with the collaboration of ALBA staff and Dr. Daniele Mantione. Grupos consolidados grant, Basque Government (IT1503-22). The authors acknowledge the technical and human support provided by SGIker (UPV/EHU/ERDF, EU) for the TEM and AFM images. MCIN/AEI/10.13039/501 100 011 033, and European Union NextGenerationEU/PRTR.

Conflict of Interest

The authors declare no conflict of interest.

Author Contributions

A.L. and L.P.F. contributed equally to this work. A.L. performed as main investigator, formal analysis, and writing-original draft. L.P.F. performed the conceptualization, investigation, formal analysis, methodology, writing-original draft, and supervision. H.S. performed conceptualization, supervision, writing – review & editing, funding acquisition, project administration, formal analysis, and methodology. I.C. performed conceptualization, formal analysis, methodology, supervision, funding acquisition, and project administration. C.M., X.L.-P., G.S., and M.C. performed an investigation. D.M.Z. performed investigation and methodology. G.P. performed the investigation and methodology. M.X.C. performed visualization and methodology. I.C. and R.A. performed an investigation and funding acquisition.

Data Availability Statement

The data that support the findings of this study are available from the corresponding author upon reasonable request.

Keywords

adhesive, click chemistry, pressure-sensitive, switchable, thiol-ene

Received: July 16, 2024
Revised: September 16, 2024
Published online: October 7, 2024

[1] Z. Liu, F. Yan, *Adv. Sci.* **2022**, *9*, 2200264.
[2] K. Imato, K. Momota, N. Kaneda, I. Imae, Y. Ooyama, *Chem. Mater.* **2022**, *34*, 8289.
[3] S. Huang, J. Sun, H. K. Bisoyi, Y. Tao, J. Wang, Y. Xu, Y. Huang, M. Wang, H. Yang, Q. Li, *Chem. Mater.* **2023**, *35*, 3705.
[4] C. Wang, X. Gao, F. Zhang, W. Hu, Z. Gao, Y. Zhang, M. Ding, Q. Liang, *Small* **2022**, *18*, 2200336.
[5] M. Kim, H. Lee, M. C. Krecker, D. Bukharina, D. Nepal, T. J. Bunning, V. V. Tsukruk, *Adv. Mater.* **2021**, *33*, 2103674.
[6] W. Li, L. Jiang, S. Wu, S. Yang, L. Ren, B. Cheng, J. Xia, *Small* **2022**, *18*, 2107544.
[7] C. Heinzmann, C. Weder, L. M. De Espinosa, *Chem. Soc. Rev.* **2016**, *45*, 342.
[8] S. Sun, M. Li, A. Liu, *Int. J. Adhes.* **2013**, *41*, 98.
[9] S. McCreath, P. Boinard, E. Boinard, P. Gritter, J. J. Liggat, *Int. J. Adhes. Adhes.* **2022**, *117*, 103168.
[10] P. Jojibabu, Y. X. Zhang, A. N. Rider, J. Wang, R. Wuhrer, B. G. Prusty, *Int. J. Adhes. Adhes.* **2020**, *98*, 102521.
[11] A. Nishiguchi, S. Ito, K. Nagasaka, T. Taguchi, *ACS Appl. Bio Mater.* **2022**, *5*, 4932.
[12] W. Cui, R. Zhu, Y. Zheng, Q. Mu, M. Pi, Q. Chen, R. Ran, *J. Mater. Chem. A* **2021**, *9*, 9706.
[13] M. Li, H. Lu, M. Pi, H. Zhou, Y. Wang, B. Yan, W. Cui, R. Ran, *Adv. Sci.* **2023**, *10*, 2304780.
[14] X. Lopez de Pariza, P. Fanlo, L. Polo Fonseca, A. Ruiz de Luzuriaga, H. Sardon, *Prog. Polym. Sci.* **2023**, *145*, 101735.
[15] E. Delebecq, J.-P. P. Pascault, B. Boutevin, F. Ganachaud, *Chem. Rev.* **2013**, *113*, 80.
[16] M. D. Konieczynska, M. W. Grinstaff, *Acc. Chem. Res.* **2017**, *50*, 151.
[17] S. H. Jung, G. Choi, S. Jeong, J. Park, H. Yoon, J. J. Park, H. Kim, *ACS Sustainable Chem. Eng.* **2022**, *10*, 13816.
[18] J. Zhou, Q. Y. Zhang, S. J. Chen, H. P. Zhang, A. J. Ma, M. L. Ma, Q. Liu, J. J. Tan, *Polym. Test.* **2013**, *32*, 608.
[19] S. Beigi, H. Yeganeh, M. Atai, *Dent. Mater.* **2013**, *29*, 777.
[20] B. Oberleitner, A. Dellinger, A. S. Castanet, A. Galtayries, V. Semetey, *Chem. Commun.* **2013**, *49*, 1615.
[21] S. Cespedes, R. A. Hand, N. Chmel, G. Moad, D. J. Keddie, T. L. Schiller, *Eur. Polym. J.* **2021**, *151*, 110440.
[22] S. P. S. Koo, M. M. Stamenović, R. Arun Prasath, A. J. Inglis, F. E. D. U. Prez, C. Barner-Kowollik, W. I. M. Van Camp, T. T. Junkers, *J. Polym. Sci. Part A Polym. Chem.* **2010**, *48*, 1699.
[23] B. G. Rutherglen, R. A. McBath, Y. L. Huang, D. A. Shipp, *Macromolecules* **2010**, *43*, 10297.
[24] P. Derboven, D. R. D'Hooge, M. M. Stamenovic, P. Espeel, G. B. Marin, F. E. Du Prez, M. F. Reyniers, *Macromolecules* **2013**, *46*, 1732.
[25] J. Kamada, K. Koynov, C. Corten, A. Juhari, J. A. Yoon, M. W. Urban, A. C. Balazs, K. Matyjaszewski, *Macromolecules* **2010**, *43*, 4133.
[26] W. Li, I. B. Baldus, F. Gräter, *J. Phys. Chem. B* **2015**, *119*, 5386.
[27] B. Zhang, P. Chakma, M. P. Shulman, J. Ke, Z. A. Digby, D. Konkolewicz, *Org. Biomol. Chem.* **2018**, *16*, 2725.
[28] B. Zhang, Z. A. Digby, J. A. Flum, P. Chakma, J. M. Saul, J. L. Sparks, D. Konkolewicz, *Macromolecules* **2016**, *49*, 6871.
[29] O. Llorente, A. Agirre, I. Calvo, M. Olaso, R. Tomovska, H. Sardon, *Polym. J.* **2021**, *53*, 1195.
[30] J. Sinha, S. Soars, C. N. Bowman, *Macromolecules* **2021**, *54*, 1693.
[31] K. Cheng, A. Chortos, J. A. Lewis, D. R. Clarke, *ACS Appl. Mater. Interfaces* **2022**, *14*, 4552.
[32] S. Chatani, T. Gong, B. A. Earle, M. Podgórski, C. N. Bowman, *ACS Macro Lett.* **2014**, *3*, 315.
[33] M. Claudino, X. Zhang, M. D. Alim, M. Podgórski, C. N. Bowman, *Macromolecules* **2016**, *49*, 8061.
[34] N. B. Cramer, C. N. Bowman, *J. Polym. Sci. Part A Polym. Chem.* **2001**, *39*, 3311.
[35] S. K. Reddy, N. B. Cramer, M. Kalvaitas, T. Y. Lee, C. N. Bowman, *Aust. J. Chem.* **2006**, 586.
[36] C. E. Hoyle, T. Y. Lee, T. Roper, *J. Polym. Sci. Part A Polym. Chem.* **2004**, *42*, 5301.
[37] C. E. Hoyle, A. B. Lowe, C. N. Bowman, *Chem. Soc. Rev.* **2010**, *39*, 1355.
[38] R. Nyquist, *Thiols, Sulfdes Disulfdes, Alkanethiols, Alkanedithiols (S-H stretching)* **2001**, *1*, 65.
[39] Q. Li, S. Ma, N. Lu, J. Qiu, J. Ye, Y. Liu, S. Wang, Y. Han, B. Wang, X. Xu, H. Feng, J. Zhu, *Green Chem.* **2020**, *22*, 7769.
[40] F. W. Lou, J. M. Xu, B. K. Liu, Q. Wu, Q. Pan, X. F. Lin, *Tetrahedron Lett.* **2007**, *48*, 8815.
[41] I. A. Lobo, P. A. Robertson, L. Villani, D. J. D. Wilson, E. G. Robertson, *J. Phys. Chem. A* **2018**, *122*, 7171.
[42] R. Acosta Ortiz, J. de J. Ku Herrera, A. O. Garcia Santos, A. E. García Valdez, G. Soria Arguello, *J. Polym. Res.* **2021**, *28*, 366.
[43] P. Science, O. Uniuersity, *Macromolecules* **1974**, *7*.

[44] R. Gan, H. Lin, J. Li, J. Huang, X. Cao, L. Qian, *J. Polym. Res.* **2023**, *30*, 314.
[45] M. Rubinstein, R. H. Colby, *Polymer Physics*, Oxford University Press, New York – Oxford, **2003**.
[46] R. G. Larson, *The Structure and Rheology of Complex Fluids*, Oxford University Press, New York – Oxford, **1999**.
[47] S. Santos, K. Gadelrab, C. Y. Lai, T. Olukan, J. Font, V. Barcons, A. Verdaguer, M. Chiesa, *J. Appl. Phys.* **2021**, *129*, 134302.
[48] R. García, R. Pérez, *Surf. Sci. Rep.* **2002**, *47*, 197.
[49] R. Pecora, *Dynamic Light Scattering: Applications of Photon Correlation Spectroscopy*, Springer, New York **1985**.
[50] R. Borsali, R. Pecora, *Soft Matter Characterization*, Springer, Dordrech **2008**.
[51] Y. Mai, A. Eisenberg, *Chem. Soc. Rev.* **2012**, *41*, 5969.
[52] S. Lecommandoux, R. Borsali, M. Schappacher, A. Deffieux, T. Narayanan, C. Rochas, *Macromolecules* **2004**, *37*, 1843.
[53] V. Abetz, P. F. W. Simon, *Adv. Polym. Sci.* **2005**, *189*, 125.
[54] N. A. Lynd, M. A. Hillmyer, *Macromolecules* **2005**, *38*, 8803.
[55] K. Kojio, S. Nozaki, A. Takahara, S. Yamasaki, *J. Polym. Res.* **2020**, *27*, 64.
[56] M. Gholami, V. Haddadi-Asl, I. S. Jouibari, *J. Plast. Film Sheeting* **2022**, *38*, 502.
[57] R. W. Clarke, M. R. Caputo, L. Polo Fonseca, M. L. McGraw, L. T. Reilly, K. A. Franklin, A. J. Müller, E. Y. X. Chen, *J. Am. Chem. Soc.* **2024**, *146*, 4930.
[58] R. Anderson, R. Buscall, R. Eldridge, P. Mulvaney, P. Scales, *RSC Adv.* **2014**, *4*, 46876.
[59] M. Kamperman, A. Synytska, *J. Mater. Chem.* **2012**, *22*, 19390.
[60] R. Hensel, K. Moh, E. Arzt, *Adv. Funct. Mater.* **2018**, *28*, 1800865.
[61] Y. Wang, D. Liu, C. Wang, J. Wu, X. Xu, X. Yang, C. Sun, P. Jiang, X. Wang, *Chem. Eng. J.* **2023**, *457*, 141268.
[62] S. Wang, H. Luo, C. Linghu, J. Song, *Adv. Funct. Mater.* **2021**, *31*, 2010297.
[63] Z. Yang, Y. He, Y. Ma, L. Li, Y. Wang, *Adv. Funct. Mater.* **2022**, *33*, 2213150.
[64] X. Shi, P. Wu, *Small* **2021**, *17*, 2101220.
[65] L. Liu, Z. Liu, Y. Ren, X. Zou, W. Peng, W. Li, Y. Wu, S. Zheng, X. Wang, F. Yan, *Angew. Chemie – Int. Ed.* **2021**, *60*, 8948.
[66] A. Sierra-Romero, K. Novakovic, M. Geoghegan, *Angew. Chemie – Int. Ed.* **2024**, *63*, 202310750.